Final Technical Report

For the Project:

The Influence of Cloud Microphysics and Radiation on the Response of Water Vapor and Clouds to Climate Change

Supported by:

U.S. Department of Energy
Office of Science
Office of Biological and Environmental Research
Climate and Environmental Sciences Division
Regional and Global Climate Modeling Program
DOE Technical Contact: Dr. Renu Joseph, RGCM Program Manager

DOE Grant Numbers: DE-FG02-07ER64465 and DE-FG02-07ER64466

Prepared by:

Dr. Kerry Emanuel, Principal Investigator
Massachusetts Institute of Technology
77 Massachusetts Avenue, Cambridge, Massachusetts 02139-4307
Tel: 617-253-2462; Fax: 617-324-0308; E-mail: emanuel@mit.edu

and

Michael J. Iacono, Principal Investigator
Atmospheric and Environmental Research, Inc.
131 Hartwell Avenue, Lexington, Massachusetts 02421-3126
Tel: 781-761-2288; Fax: 781-761-2299; E-mail: miacono@aer.com

For the Project Period:
15 August 2007 - 14 August 2010

11 November, 2010

Table of Contents

1. Overview

Uncertainties in representing the atmospheric water cycle are major obstacles to an accurate prediction of future climate. This project focused on addressing some of these uncertainties by implementing new physics for convection and radiation into the NCAR climate model. To better understand and eventually better represent these processes, we modified CAM3.5 to use the convection and cloud schemes (*Emanuel and Zivkovic-Rothman,* 1999; *Bony and Emanuel*, 2001) developed by the Massachusetts Institute of Technology (MIT) and the RRTMG rapid radiation code for global models (*Iacono et al.,* 2008) developed by Atmospheric and Environmental Research, Inc. (AER). The impact of the new physics on the CAM3.5 simulation of convection on diurnal and intra-seasonal scales, intra-seasonal oscillations and the distribution of water vapor has been investigated. The effect of the MIT and AER physics also has been tested in the Weather Research and Forecasting (WRF) regional forecast model.

It has been found that the application of the AER radiation and MIT convection produces significant improvements in the modeled diurnal cycle of convection, especially over land, in the NCAR climate model. However, both the standard CAM3.5 (hereinafter STD) and the modified CAM3.5 with the new physics (hereinafter MOD) are still unable to capture the proper spectrum and propagating characteristics of the intra-seasonal oscillations (ISOs). The new physics methods modify, but do not substantially improve, the distribution of upper tropospheric water vapor relative to satellite measurements. The major results that are summarized in this report have been described in more detail in a journal article titled "The Impacts of AER Radiation and MIT Convection on the Water Cycle Simulated by CAM3.5" (*Yang et al.,* 2010) that will be submitted for publication during Fall 2010.

2. Diurnal Variation of Convection

A pair of multi-year, ensemble experiments were performed that followed the Atmospheric Model Intercomparison Project (AMIP) protocol and used prescribed sea surface temperatures for the period 1992-1997. The first ensemble experiment used the STD model; the second one used the MOD version of CAM3.5 with the new physics as described in the previous section. Each ensemble experiment consisted of five ensemble members, and each simulation utilized the CAM finite volume dynamic core running on 1.9 deg x 2.5 deg horizontal resolution. To accommodate the new convection model, the vertical resolution in the ensemble experiment with MOD was made finer in the middle and upper troposphere by increasing the number of layers to 47 from the default configuration of 26 layers used in STD.

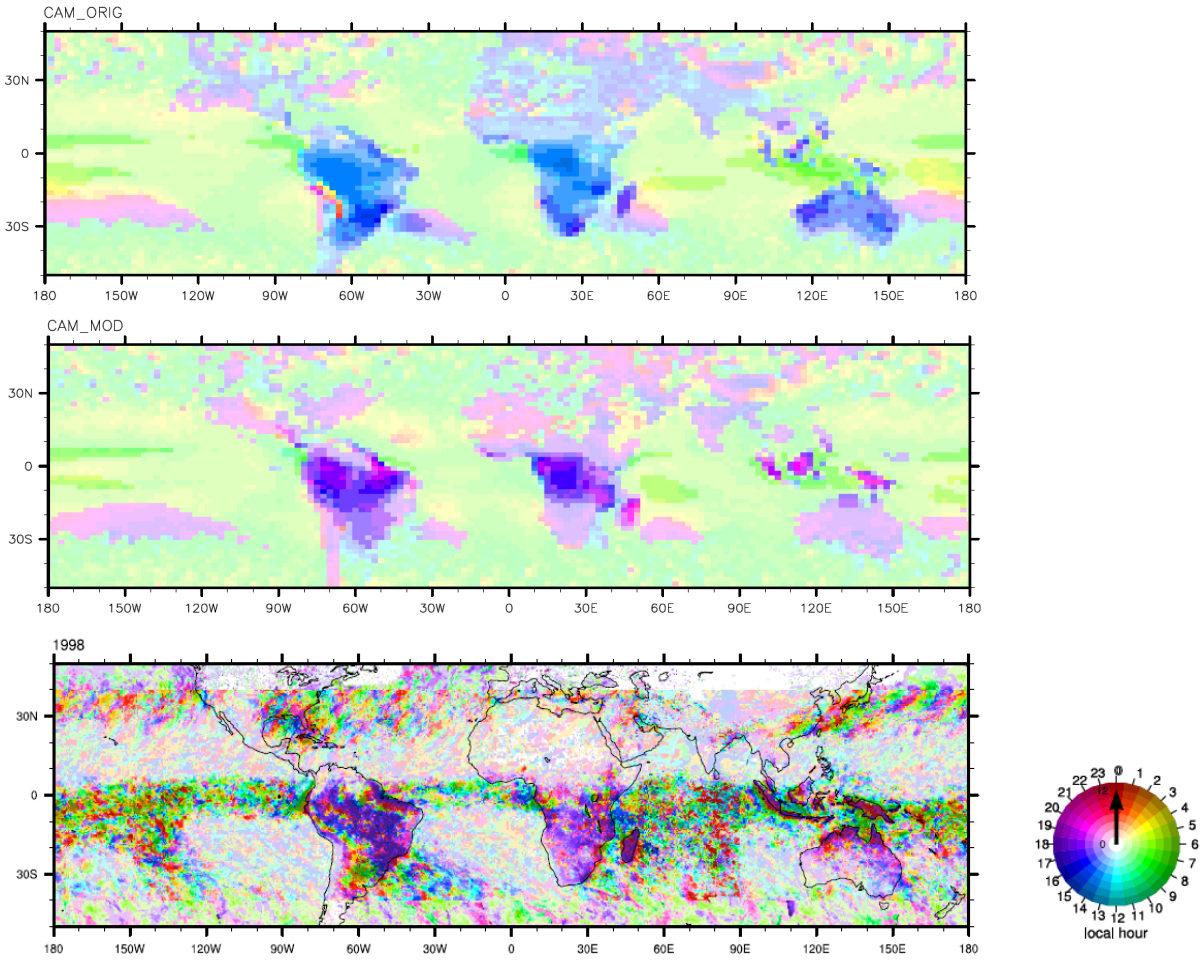

Figure 1. The phase (local standard time in hours of the maximum) and amplitude of the 24-hr harmonic estimated from the mean diurnal anomalies of modeled DJF precipitation before (upper panel) and after (middle panel) the implementation of the AER radiation and the MIT convection and clouds. The lower panel shows the TRMM observation. The phase-hour color scale is shown at lower right, and amplitude is indicated by the color saturation.

The phase (local solar time, hereinafter LST) and amplitude of the diurnal precipitation maximum for two ensemble simulations and the TRMM observations are shown for boreal winter in Figure 1. The time of day of the precipitation maximum (phase) is indicated by the color scale at lower right in Figure 1, and amplitude is indicated by the saturation of each color. In general, the observed precipitation diurnal cycle is stronger over land than over the open ocean. The large amplitude over the ocean only occurs near the intertropical convergence zone (ITCZ) and the South Pacific convergence zone (SPCZ), where the total precipitation amount is also large. Consistent with previous findings, the diurnal precipitation is characterized by the late-evening to early-morning maximum over the open oceans and the middle to late afternoon maximum over most of the tropical land areas.

The standard CAM3.5 generally produces maximum precipitation over land near or just after noon (LST), which is a few hours earlier than observations. Such biases have been largely rectified in the experiment with the modified CAM3.5. The seasonal shift of the diurnal cycle is also well simulated. However, the amplitude of the diurnal cycle at ITCZ (and SPCZ) is still weaker compared with that of the observations, though the phase lag between ITCZ (and SPCZ) and its surrounding area has been roughly captured. Given the coarse resolution of the model, the modified CAM3.5 does a rather decent job simulating the tropical precipitation diurnal cycle.

As the largest tropical forest and one of the heaviest rainfall regions on the earth, the Amazon basin is an excellent site for investigating the diurnal variations of the hydrological cycle from the perspective of land-surface-atmosphere interactions. The TRMM-wet season atmosphere meso-scale campaign (WETAMC)/large-scale Biosphere-Atmosphere (LBA) Experiment was conducted over this region during January and February 1999 (*Betts,* 2002). It combined various space-borne and surface-based measurements to provide an excellent dataset for evaluating the modeled diurnal cycle over a typical land convection area.

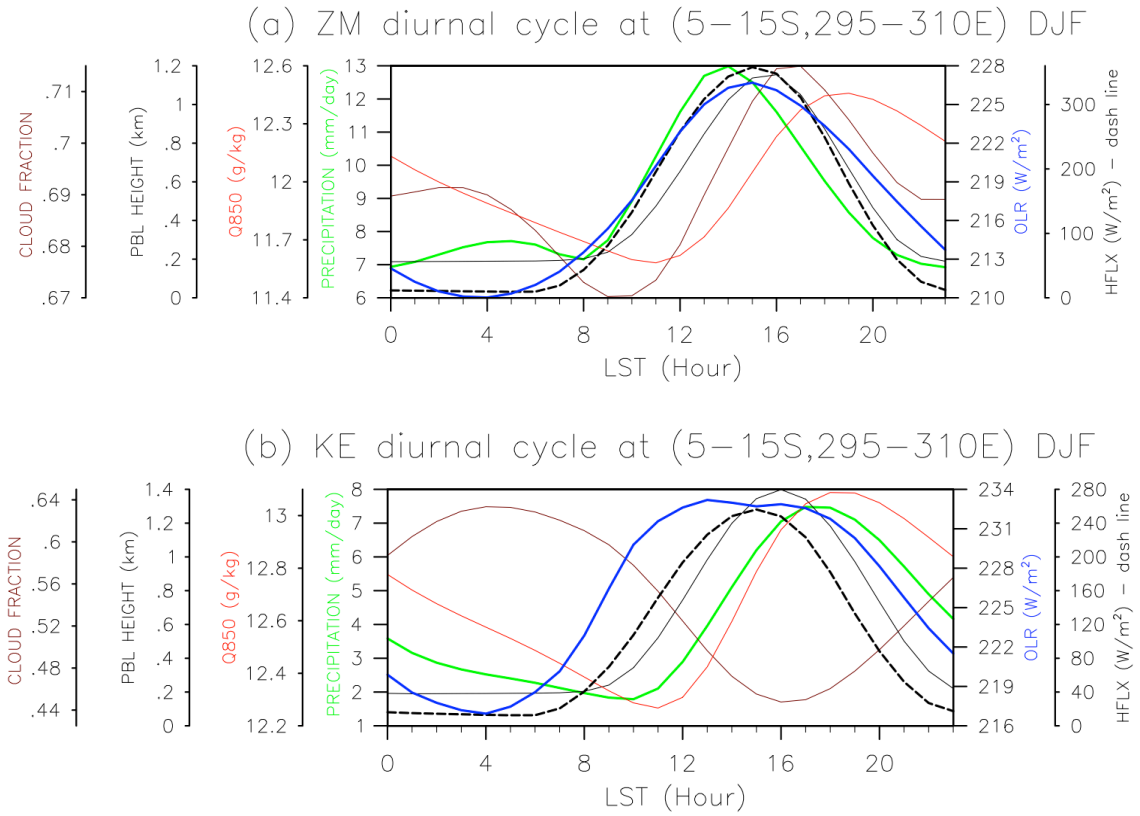

Figure 2. Mean diurnal cycle of precipitation (green line, mm day^{-1}), OLR (blue line, W m^{-2}), latent heat flux (black dash line, W m^{-2}), PBL height (black line, km), and cloud fraction (brown line) averaged over the Amazon area within $5^o - 15^o S,\ 295^o - 310^o E$ in the standard (a) and modified (b) CAM3.5.

Over the Amazon basin, the MOD produces a diurnal cycle that is in better agreement with the observations. Measured rainfall indicates a daily minimum in the morning (0900-1000 LST) and a daily maximum in the afternoon (1500-1600 LST) (*Lin et al.,* 2000); whereas the MOD has a rainfall maximum at 1700 LST and a minimum at 1000 LST (Figure 2b). In MOD, the OLR increases rapidly after sunrise. The pick-up of the surface latent heat flux follows that of the OLR, but with a two-hour delay. The PBL heights increase rapidly from 0800 LST to 1600 LST, lagging the growth of surface latent heat flux by about one hour. Finally, the precipitation pick-up further lags that of the PBL height by another two hours. The phase of the latent heat and PBL height in STD are almost identical to those in MOD. However, the precipitation pick-up occurs much earlier, roughly in phase with OLR and the surface latent hear flux (Figure 2a), suggesting that the implementation of the MIT convection and cloud schemes might be responsible for preventing the early realization of the peak precipitation.

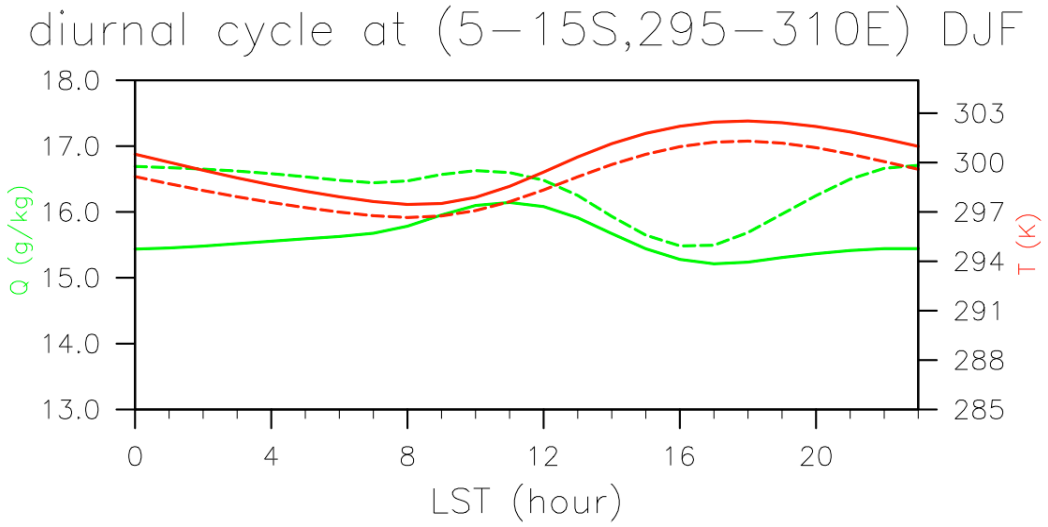

Figure 3. DJF mean diurnal cycle of air temperature (red) and specific humidity (green) at the lowest model level (σ = 0.9926) averaged over the Amazon area within 5°-15°S, 295°-310°E in the modified (solid line) and standard (dash line) CAM3.5.

The unsaturated downdrafts driven by the evaporation of precipitation are important agents of the coupling between boundary layer and troposphere and are crucial for re-stabilizing the sub-cloud layer (*Emanuel*, 1991). The *Zhang and McFarland* (1995) convection scheme in STD only has a saturated downdraft. In contrast, the Emanuel scheme in MOD has both saturated and unsaturated downdrafts. Note that q in MOD is always lower and T is always larger than that in STD, suggesting a much drier surface layer in the former. By maintaining a relatively dry sub-cloud layer (Figure 3), the unsaturated downdraft could possibly play a role in preventing the early realization of the peak precipitation. To test this hypothesis, experiments with the single column version of the Emanuel convection and cloud schemes have been performed. In "weak

temperature gradient" mode, wherein the temperature above the boundary layer is not permitted to vary in time, the experiment without the unsaturated downdraft produces an afternoon precipitation maximum that is approximately two hours earlier than the experiment with the downdraft (figures not shown). However, removing the unsaturated downdrafts in the modified CAM3.5 does not generate a similar change on the timing of the diurnal precipitation maximum. The interactions among various physical processes in a 3-D full climate model are more complex than that in its single column version. More sensitivity experiments and diagnostic studies with the modified CAM3.5 and single-column version of the Emanuel convection and cloud model need to be done to identify the causes for the change of the modeled diurnal cycle.

3. Madden-Julian Oscillation

Simulations with both STD and MOD are unable to capture the coherent structures and propagating characteristics of intra-seasonal oscillations (ISOs) and of the Madden-Julian Oscillation (MJO) in particular. The ability of STD and MOD to simulate the MJO was examined using the diagnostic metrics developed by the U. S. CLIVAR MJO working group. Both STD and MOD have difficulty representing the observed magnitude and geographical distribution of MJO as evidenced by the outgoing longwave radiation (OLR) variances shown in Figure 4 (AVHRR observation), Figure 5 (standard CAM3.5), and Figure 6 (modified CAM3.5). The unfiltered modeled variances (top panels in Figures 4, 5, and 6) are generally much higher than observed. The observed unfiltered OLR variance maxima are located in the eastern Indian Ocean, western Pacific, and to the southeast of the maritime continent. Although both simulations somewhat capture this geographical distribution, the large variance areas extend too far eastward and southeastward. Similar biases are also seen in maps of the simulated 20-100 day filtered variance (center panels in Figures 4, 5, and 6). Spatial distributions of the ratio between 20-100 day filtered variance and unfiltered variance in both simulations are rather chaotic in both simulations. In contrast, the observations show a much more regular pattern with a maximum center located over the Indian Ocean.

Various attempts were made during this research to explore the sensitivity of modeled intra-seasonal oscillations to multiple parameters (e.g., the relaxation and mass flux damping rate in sub-cloud quasi-equilibrium closure, the fraction of rain shafts falling through their environment, the gustiness factor, and the mixing rate and mixing distribution between the plume and its environment) in the Emanuel (MIT) convection scheme. However, the modified climate model still could not generate the proper spectrum and coherent structures of the observed ISOs.

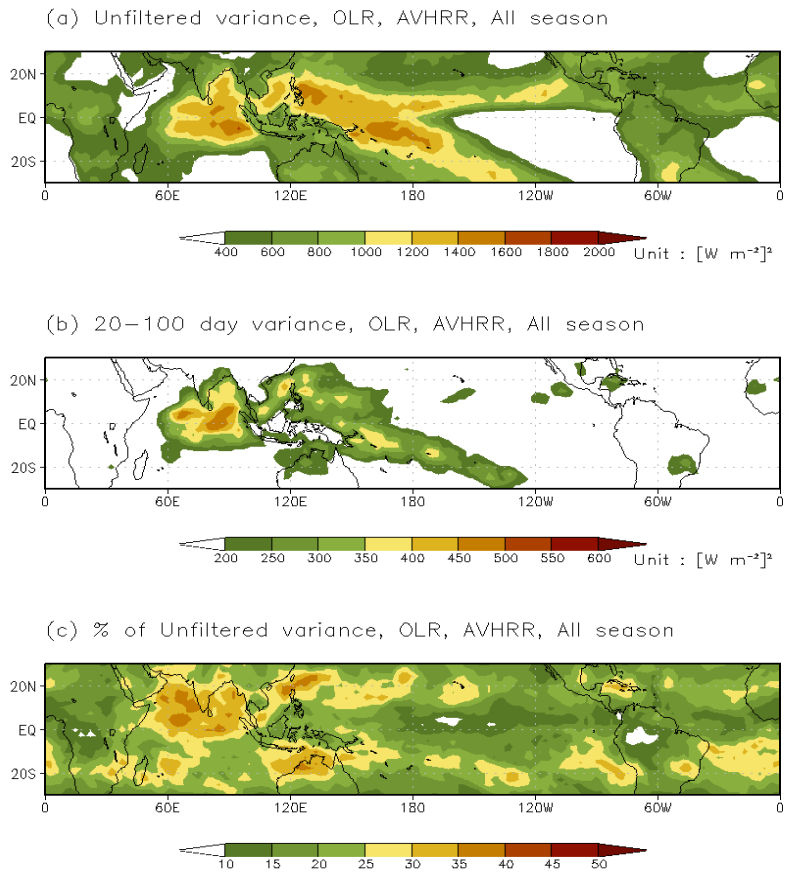

Figure 4. Variance maps of 1993-1997 advanced very high resolution (AVHRR) outgoing longwave radiation (OLR) (a) unfiltered variance, (b) 20-100 day filtered variance, (c) 20-100 day filtered variance expressed as a percent of the unfiltered variance.

It is intriguing that ISOs can be produced by theoretical and idealized models tuned to represent certain simplified mechanisms, but not by most global climate models (GCMs) even with their more sophisticated treatments of physical processes. It could be argued that what is in the idealized models but missing from the GCMs would make the MJO present in the former and absent in the latter. However, for the current implementations, it is more likely that the key processes that are vital to the ISOs are present in GCMs, but are either altered, interrupted, or compensated through complex interactions with other parameterized physical processes. To target this problem, more attention has to be paid to the interactions and consistency among different physical parameterization processes in the future.

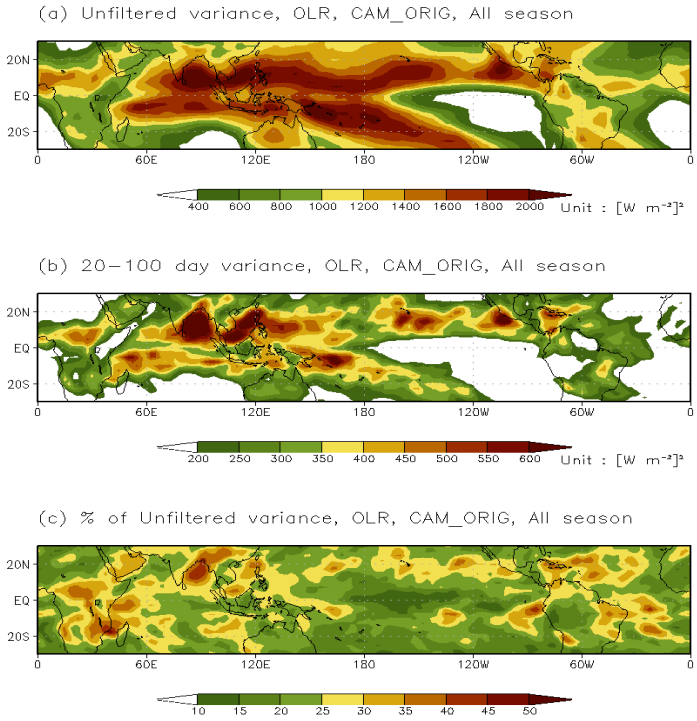

Figure 5. As in Figure 4 but for OLR variance in the standard (STD) CAM3.5.

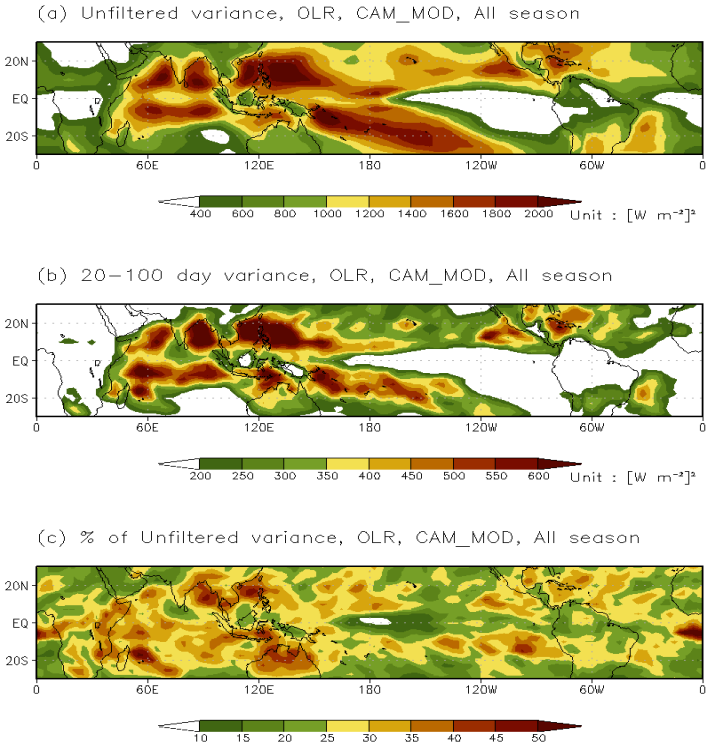

Figure 6. As in Figure 4 but for OLR variance in the modified (MOD) CAM3.5.

4. RRTMG Radiation

Development of the AER radiative transfer model for GCMs, RRTMG (*Iacono et al.,* 2008), as well as its implementation and testing in various dynamical models, have proceeded under separate support from the DOE Atmospheric System Research (ASR) Program (formerly the Atmospheric Radiation Measurement Program). This radiation model is available to the scientific community through the AER radiative transfer web site (www.rtweb.aer.com). NCAR has adopted RRTMG as the new radiation model in CAM5 and CESM1, which were released in June 2010. It is expected that some of the planned IPCC simulations for the 5th Assessment Report (AR5) will be performed with CAM5/CESM1, although the majority are being performed with CAM4/CCSM4. RRTMG has also been implemented as new longwave and shortwave radiation options in the Weather Research and Forecasting (WRF) model as of version 3.1, which was released in April 2009. Additional global models are using or testing the RRTMG radiation including those maintained by the European Centre for Medium-Range Weather Forecasts, the National Centers for Environmental Prediction, the Max Planck Institute, and the NASA Goddard Space Flight Center.

Other significant changes between CAM3.5 and the previous version that might impact this analysis include changes in the planetary boundary layer and cloud microphysics and the use of the finite volume dynamical core (at 2.5 x 1.9 degree horizontal resolution) with a time step of 30 minutes rather than the Eulerian dynamical core (at 2.8 x 2.8 degree resolution) with a time step of 20 minutes applied in earlier tests. An additional difference between the present experiments and those described by *Iacono et al.* (2003) is the current application of the AER shortwave model in CAM3.5 and the use of the Monte-Carlo Independent Column Approximation (McICA) technique to represent sub-grid cloud variability, whereas the previous work utilized only RRTMG_LW without the McICA feature.

5. HIRS Brightness Temperature Diagnostic

This work extends earlier research to evaluate the simulation of water vapor in CAM (and its predecessor, CCM) through the comparison of modeled and observed HIRS brightness temperatures in a channel sensitive to middle and upper tropospheric water (*Iacono et al.,* 2003). Iacono et al. (2003) showed that significant discrepancies in upper tropospheric water vapor were present in some regions and time periods in both CCM3 and CAM3.0. A similar analysis has been completed with the standard and modified versions of CAM3.5 to establish whether the water discrepancies still persist in this climate model. The HIRSRTM diagnostic package

(*Engelen and Stephens*, 1999) was used to generate outgoing brightness temperatures at the top of the atmosphere in multiple HIRS channels. Specifically, we utilized output for HIRS channel 4 (CH04: 675-732 cm^{-1}) to analyze tropospheric temperature and output for HIRS channel 12 (CH12: 1382-1572 cm^{-1}) to analyze upper tropospheric water vapor. Note also that in the modified CAM3.5 we used McICA to represent partial cloudiness in the AER radiation code with the maximum-random cloud overlap assumption. Maximum-random cloud overlap, which presumes maximum vertical correlation among contiguous cloudy layers and random vertical correlation between non-contiguous blocks of clouds, is consistent with the approach used in most modern GCMs.

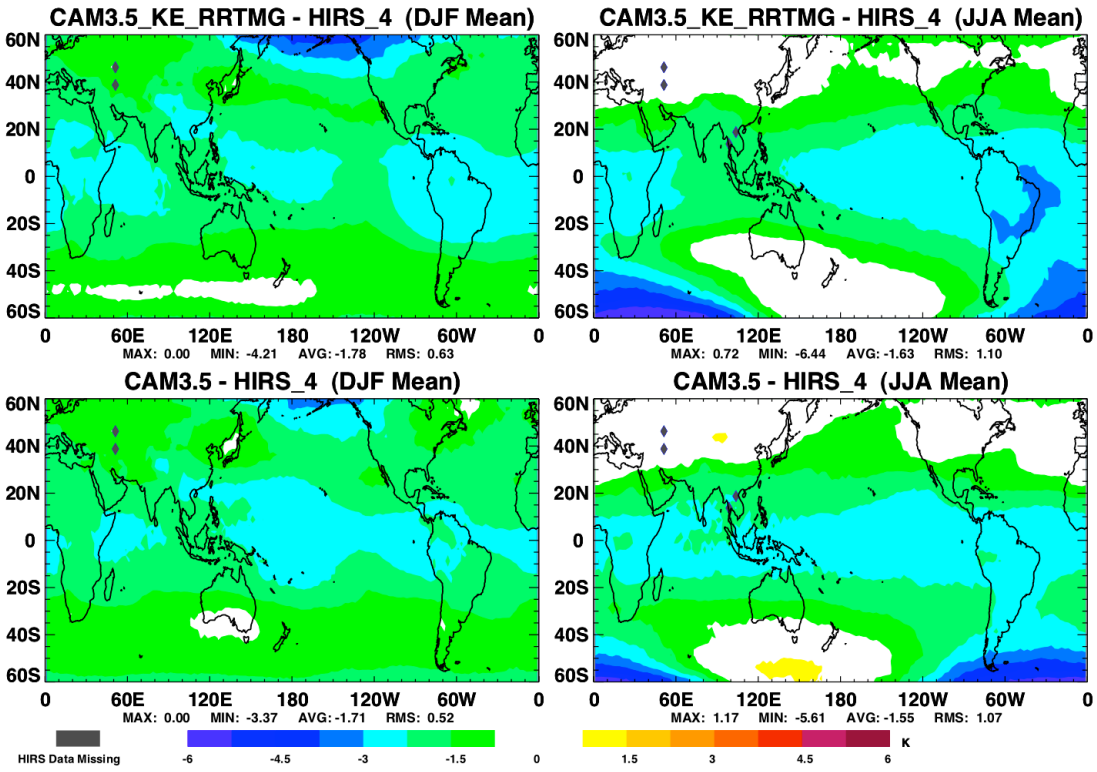

Figure 7. Differences between model simulated and HIRS observed channel 4 clear-sky brightness temperatures. Units are in K. See text for detailed explanation.

These experiments show that the HIRS channel 12 brightness temperature (BT) discrepancies previously documented for CCM3 (*Iacono et al.,* 2003) and earlier versions of CAM are still present in CAM3.5 with the AER and MIT physics. Following our earlier uses of this diagnostic, we first compare the observed and simulated HIRS CH04 brightness temperatures to quantify the effect of temperature differences and deficiencies in cloud filtering in the CH12 diagnostic. Figure 7 shows BT differences in CH04 between model and measurement for the modified CAM3.5 (top) and standard CAM3.5 (bottom) for DJF (left) and

JJA (right). Modeled results are averaged over a five-member ensemble, and both model and the HIRS data are averaged over the five-year period from 1993-1997. We find that differences in this channel are on the order of 1-2 K in the low and middle latitudes. On the other hand, in the water vapor HIRS channel (CH12) we find much larger BT differences of 6-8 K in some regions, which suggest areas where the distribution of water vapor in the model is significantly different from observed. Figure 8 shows the BT differences as in Figure 7 but for CH12. Positive (negative) differences are regions where the model result is warmer (colder) and therefore drier (wetter) than the observed atmospheric conditions in this time period. Note that the CH12 BT differences are much larger in some regions than those seen in CH04, which indicates that although CH12 is sensitive to both water vapor and temperature the larger CH12 differences are primarily due to deficiencies in the water vapor distribution. This analysis reinforces the need for continuing analysis of the causes of these significant discrepancies in upper tropospheric water vapor in this climate model. Figure 8 also illustrates that replacing the convection and radiation physics in CAM3.5 alters the water vapor distribution.

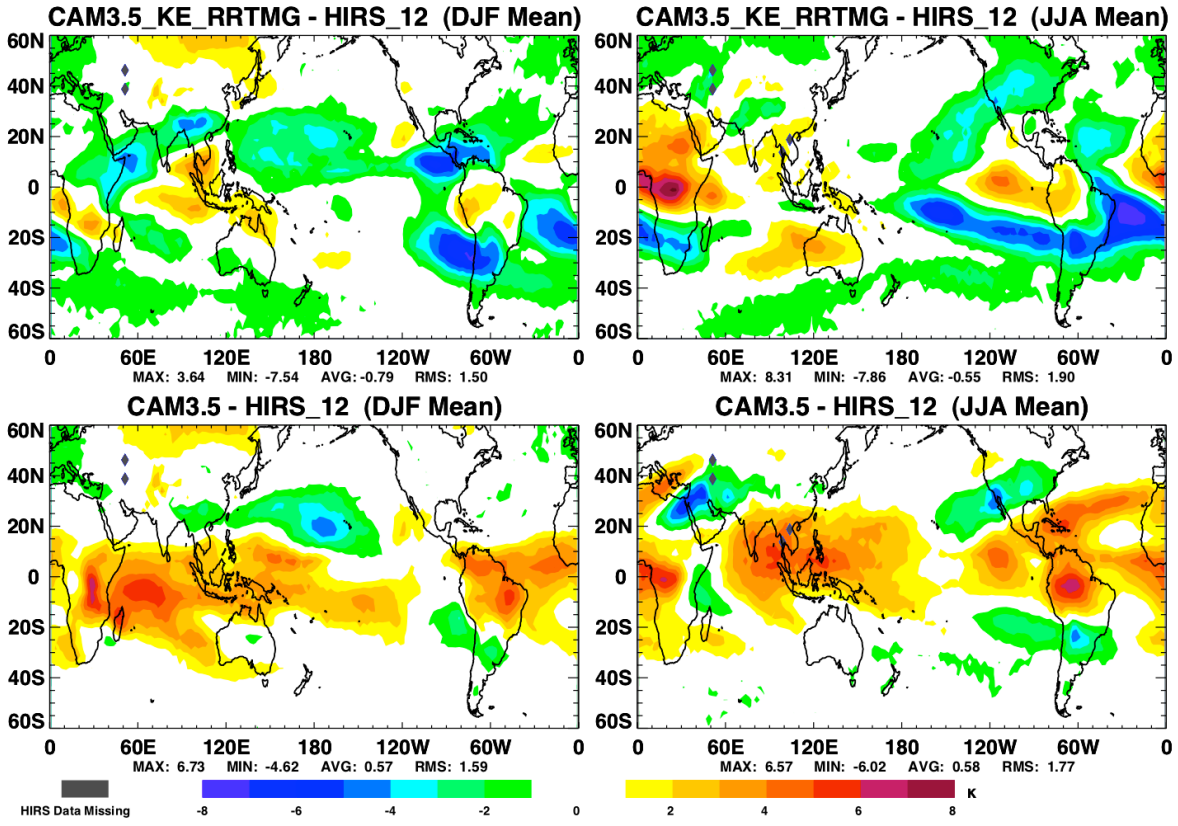

Figure 8. Differences between model simulated and HIRS observed channel 12 clear-sky brightness temperatures,. Units are in K. See text for detailed explanation.

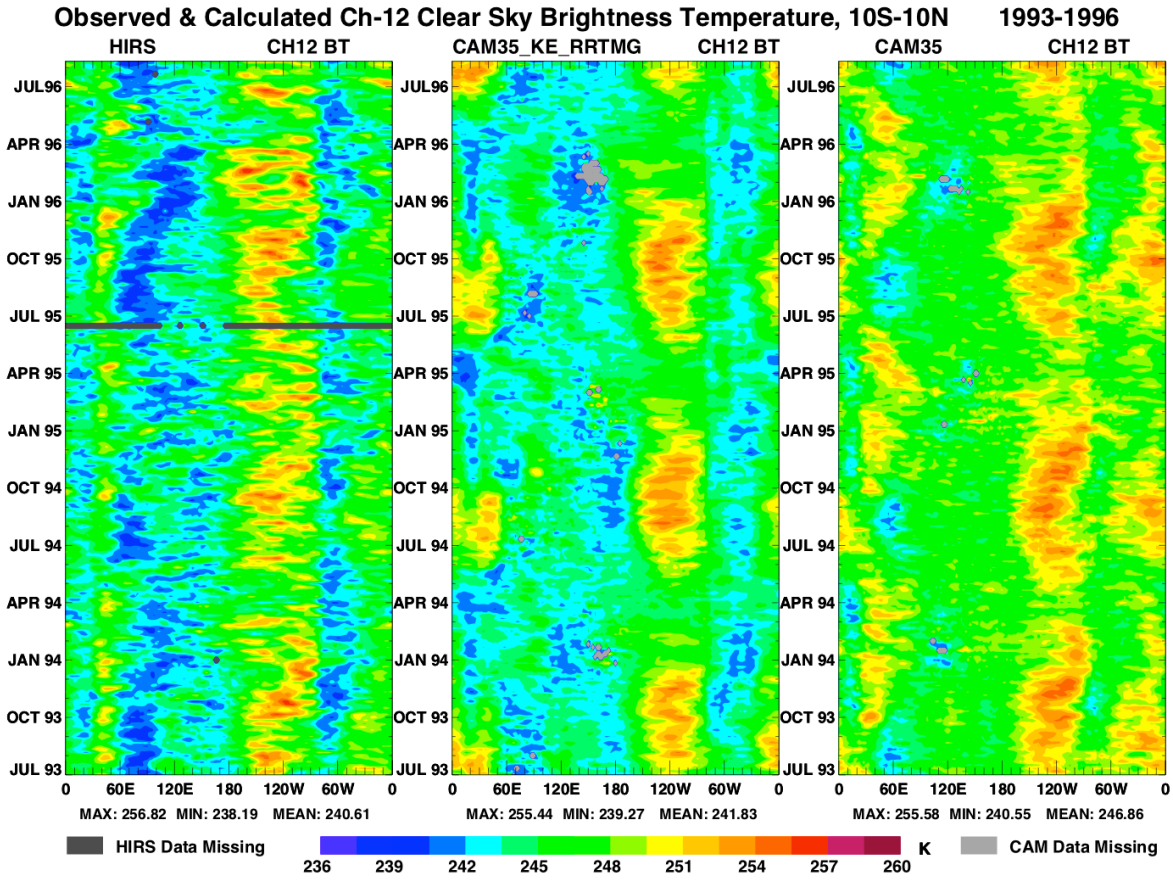

Figure 9. Diagrams of 5-day averaged clear-sky HIRS channel 12 brightness temperature averaged over the 10S-10N latitude band as observed by HIRS (left), modeled by CAM3.5 with the MIT convection and AER radiation (center) and modeled by the standard CAM3.5 (right) for July 1993 to July 1996. Units are in K.

Another perspective on the water vapor distribution can be obtained by examining the CH12 BTs by longitude as a function of time. Such diagrams illustrate the persistence, magnitude and extent of the BT differences over a longer time period. Figure 9 shows the 5-day averaged, clear-sky HIRS observed CH12 BT (left panel), and the 5-day averaged and five-member ensemble mean CH12 BT simulated by the modified CAM3.5 (center panel) and the standard CAM3.5 (right panel). Data are averaged over the 10S-10N equatorial latitude band and plotted by longitude as a function of time from July 1993 through July 1996. In each panel, warm (cold) brightness temperatures represent areas that are relatively dry (moist) in the upper troposphere. The modeled data are filtered to exclude grid points where the cloud fraction exceeds 0.3 above 700 mb. This procedure minimizes the effect of any moist bias from significantly cloudy and presumably wet profiles. In this 6.7-micron water vapor channel, the atmosphere is largely opaque below roughly 700 mb, and the presence of clouds and moisture below that level is of less consequence. Some regions (such as near India and over the western

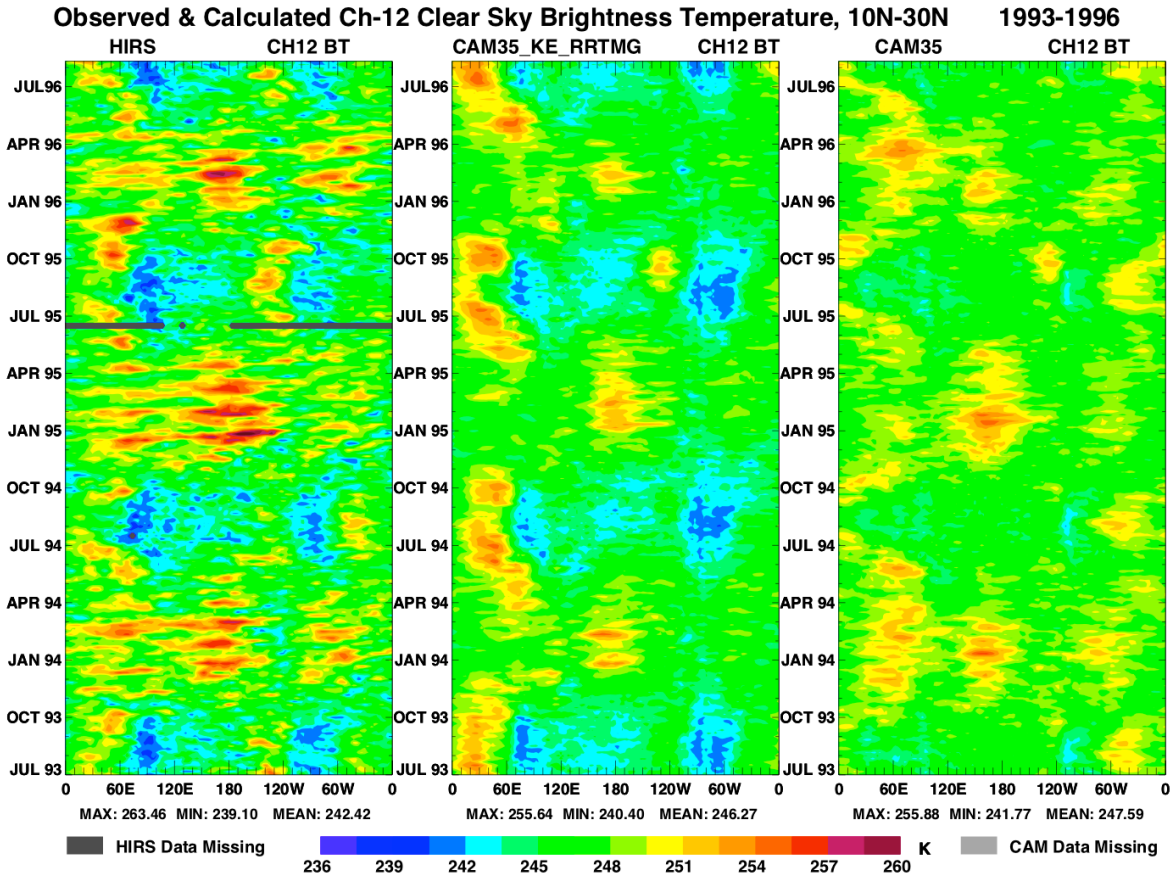

Figure 10. Diagrams of 5-day averaged clear-sky HIRS channel 12 brightness temperature averaged over the 10N-30N latitude band as observed by HIRS (left), modeled by CAM3.5 with the MIT convection and AER radiation (center) and modeled by the standard CAM3.5 (right) for July 1993 to July 1996. Units are in K.

Pacific Warm Pool) are nearly continually cloudy, and the modeled results are excluded when the sample size is small. The cold brightness temperature linear features in Figure 9 that extend from 60E-160E from July through the following July mark the progression of moisture and presumably convection eastward from near India across the western and central Pacific. Both the modified and standard CAM3.5 capture this feature to varying degrees, with the modified model generally producing CH12 BTs that are in slightly better agreement with the observation in this equatorial latitude regime. In the drier eastern Pacific, the models show more seasonal variation than observed with the wettest conditions centered in the March-May season. Figure 10 shows the same panels as Figure 9, though for BTs averaged over the latitude band from 10N-30N. Here the models are generally slightly warmer and drier than observed at most longitudes and times with the modified model producing a slightly better result. Diagonal bands of warm BT that appear in the observations (left panel of Figure 10) extend west to east across the Indian and Pacific Oceans over about 30 days during the northern winter and spring seasons. These features,

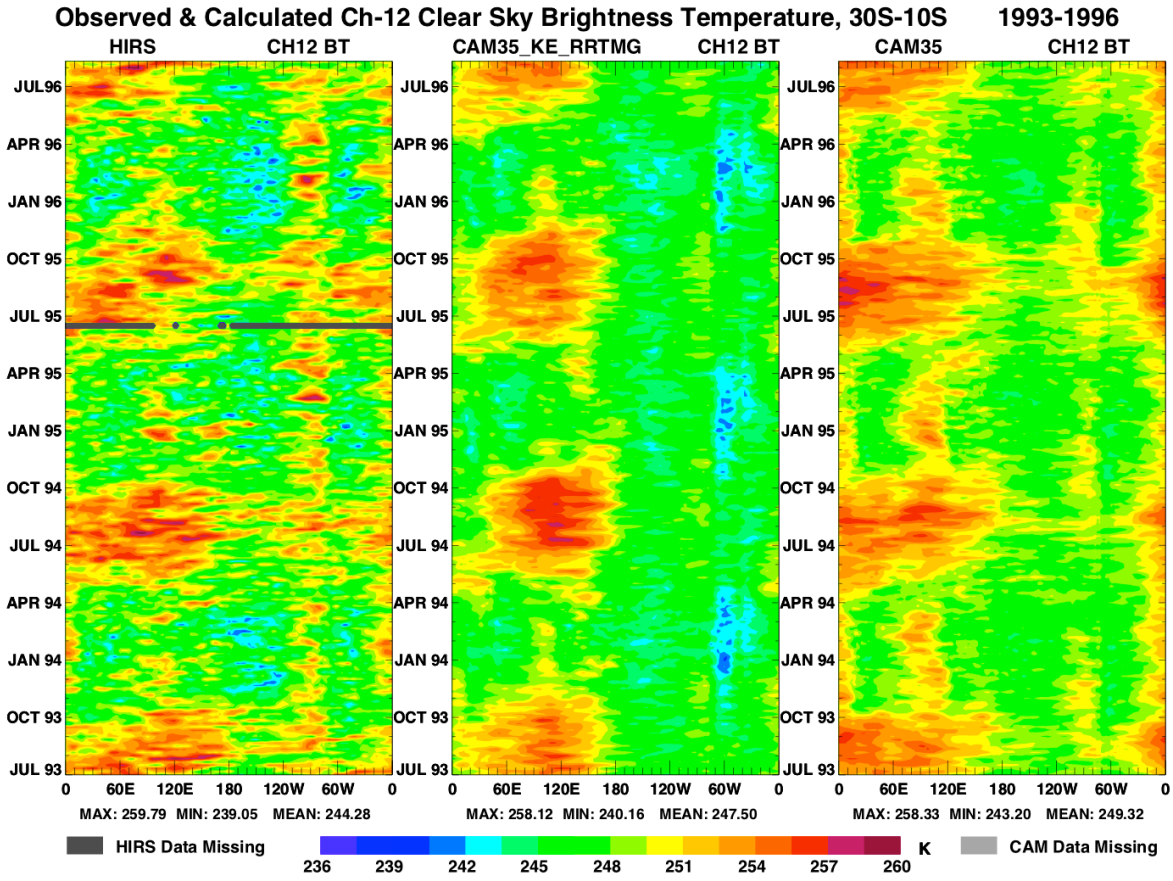

Figure 11. Diagrams of 5-day averaged clear-sky HIRS channel 12 brightness temperature averaged over the 30S-10S latitude band as observed by HIRS (left), modeled by CAM3.5 with the MIT convection and AER radiation (center) and modeled by the standard CAM3.5 (right) for July 1993 to July 1996. Units are in K.

which are suggestive of the Madden-Julian Oscillation (MJO), are much less distinct and are barely discernable in the model simulations. While the ensemble averaging utilized here is necessary to reduce the impact of model noise on the result, this may also have the effect of smoothing over some of the subtle details represented in the observations. Finally, Figure 11 shows diagrams of observed and modeled CH12 brightness temperatures averaged from 30S to 10S for July 1993 to July 1996. In this latitude band, each model simulates the seasonal cycle of CH12 BT across the Indian Ocean (40E-120E) and across the western Pacific (120E-180) relatively well. Over the central to eastern Pacific (180-80W), central South America (80W-50W) and the Atlantic Ocean (50W-0) the modified model produces brightness temperatures that are much colder and show much less seasonal variability than observed. However, when averaged over all longitudes and the full time period from July 1993 to July 1996, each model is slightly warmer (and drier) than the observation in this latitude band.

6. WRF Simulations with MIT convection and RRTMG

Due to the ongoing development of CAM during the course of this project, it was decided to advance the present research by additionally implementing the MIT convection and cloud schemes into the Weather Research and Forecasting (WRF) model (version 3.1) as an interim environment in which to investigate the roles of convection and microphysics in the context of improved radiative transfer. This implementation activity has resulted in a version of WRF that can use both the MIT and AER physics. This capability also provides an additional framework in which to evaluate the performance of the MIT convection in WRF relative to observations.

In order to illustrate the functionality of the MIT convection and cloud schemes in the WRF model, several 24-hour forecasts were performed for the period starting at 12 UTC on 24 January 2000. The model was run in two configurations, one using the MIT convection and cloud and another using the existing WRF Kain-Fritsch ETA cumulus method (convection option 1). Each simulation was performed with the RRTMG longwave and shortwave model (radiation option 4) and the WSM 3-class ice microphysics scheme (microphysics option 3). The WRF simulations covered a grid area over the Eastern United States with a grid resolution of 40-km. The MIT convection and cloud method calculates both convective and large-scale precipitation, and it has a significant impact on total precipitation for the forecast period. As shown in Figure 12, the MIT approach provides a result in closer agreement with total precipitation derived from TRMM measurements of 3-hourly precipitation rate.

The WRF model has been found to be deficient in cloud fraction in some conditions, and this situation requires further investigation, since the accuracy of radiative transfer is highly dependent on the precise specification of cloud fraction and cloud properties. Although it is being studied under separate support from the DOE ASR Program, the application of the MIT cloud and convection scheme to WRF provided an excellent opportunity to investigate this issue in the present context. The specific cause of the cloud cover deficiencies is not yet known, though the extent to which the issue is unresolved by improving radiation or convection or by varying treatments of microphysics available in WRF, suggests that the cause may be related to the atmospheric specification. Comparison of WRF simulated cloud fraction with ARM measurements over the Southern Great Plains site has shown significant deficiencies in total cloud cover regardless of the radiation model (*Iacono and Nehrkorn*, 2010). In the preliminary WRF experiments completed for this project, the MIT cumulus parameterization has been shown to have some effect on total cloud fraction (Figure 13) and on outgoing longwave radiation (Figure 14) for the 24-hour forecast period that was analyzed.

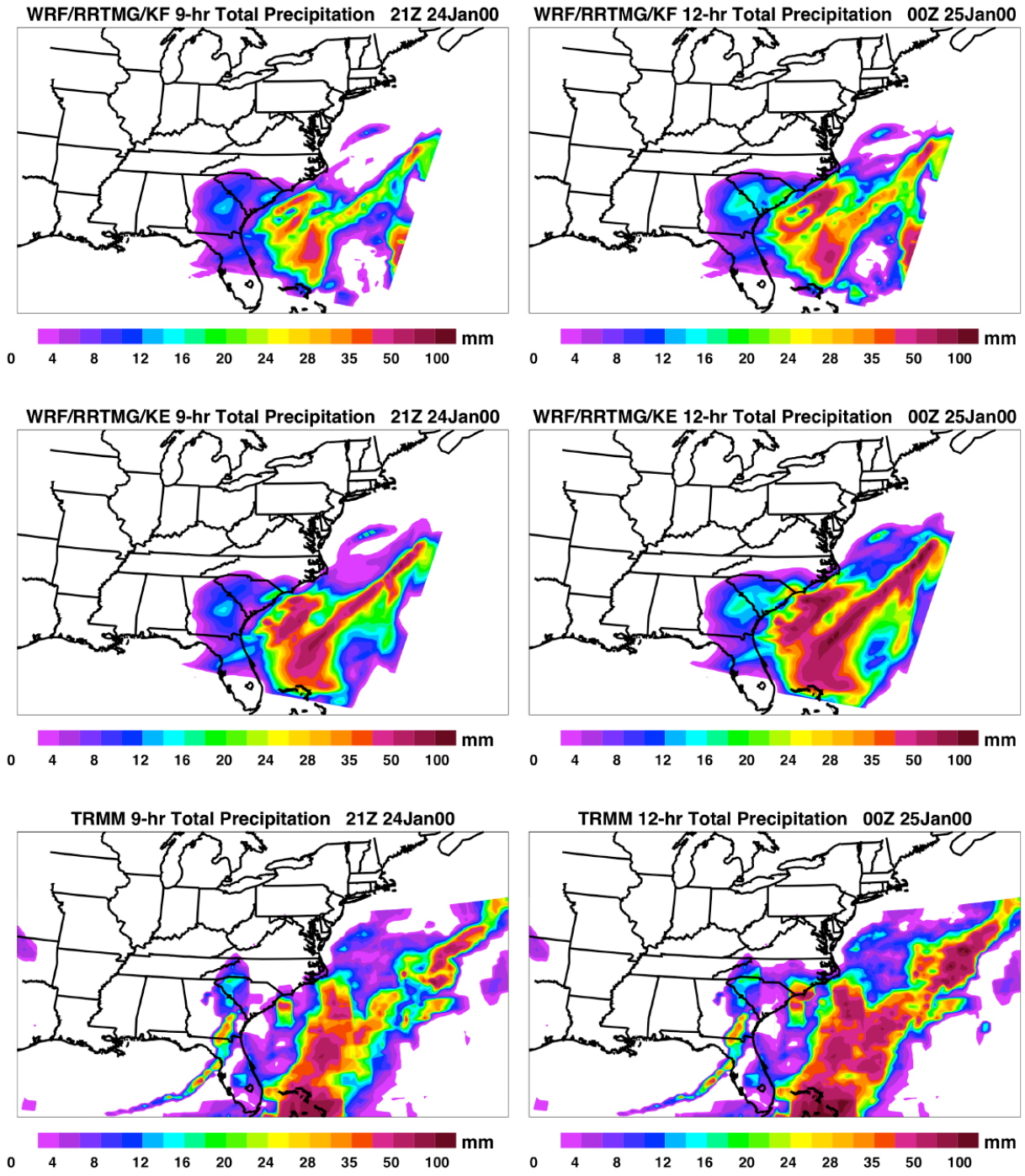

Figure 12. Accumulated precipitation (mm) for the nine hour period ending at 21 UTC 24 Jan 2000 (left) and for the 12 hour period ending at 00 UTC 25 Jan 2000 (right) as simulated by WRF using the Kain-Fritsch ETA convection (top panels), the MIT/Emanuel convection and cloud schemes (center panels) and as measured by the TRMM satellite (bottom panels). Note that the boundaries of the simulated WRF grid are smaller than the geographic area shown in each plot (see e.g. Figure 14).

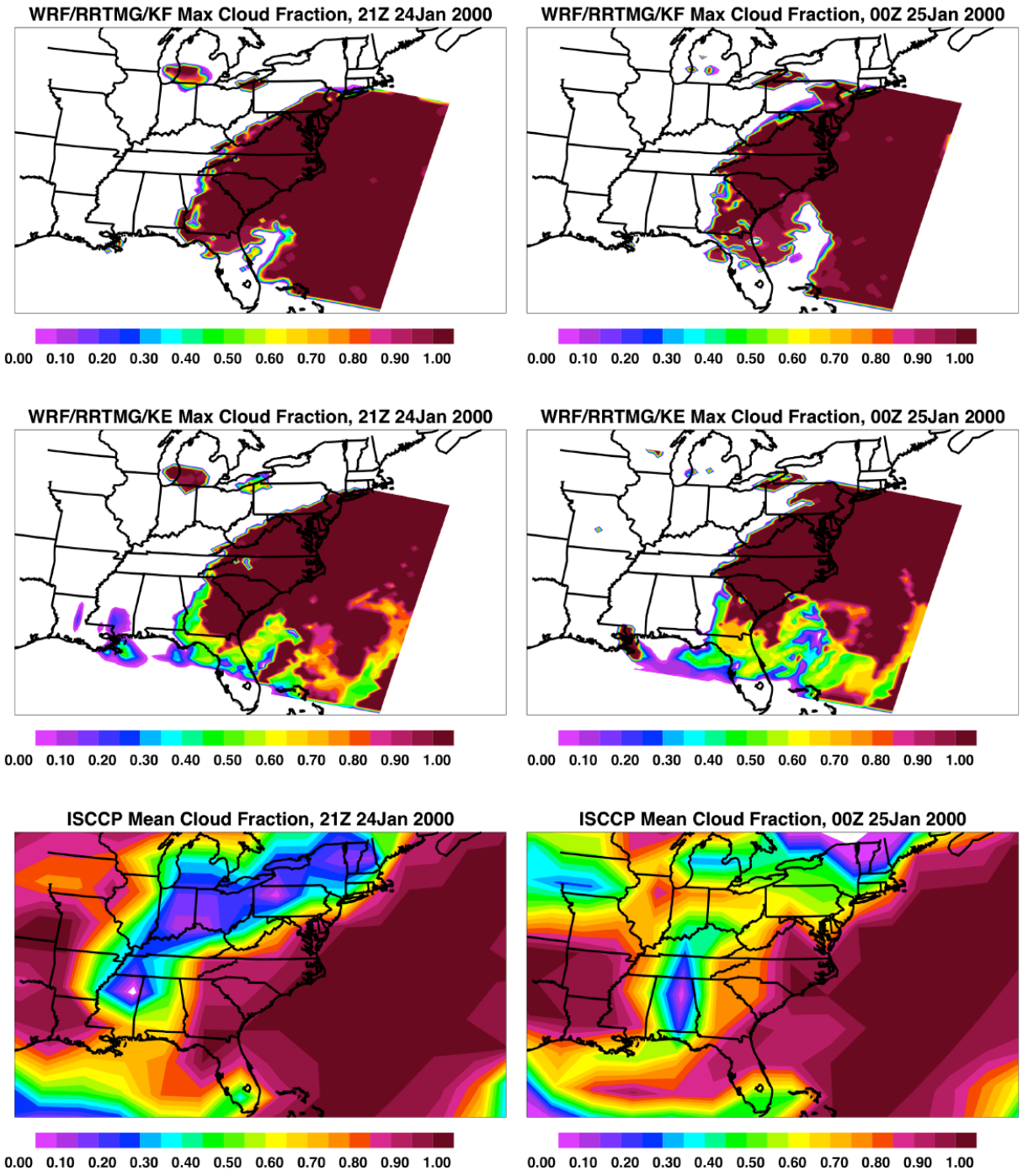

Figure 13. Maximum cloud fraction in each grid box at 21 UTC 24 Jan 2000 (left) and at 00 UTC 25 Jan 2000 (right) as simulated by WRF with the RRTMG radiation and using the Kain-Fritsch ETA convection (top panels), the MIT/Emanuel convection and cloud schemes (center panels) and mean cloud fraction measured by ISCCP (bottom panels). Note that the boundaries of the simulated WRF grid are smaller than the geographic area shown in each plot (see e.g. Figure 14).

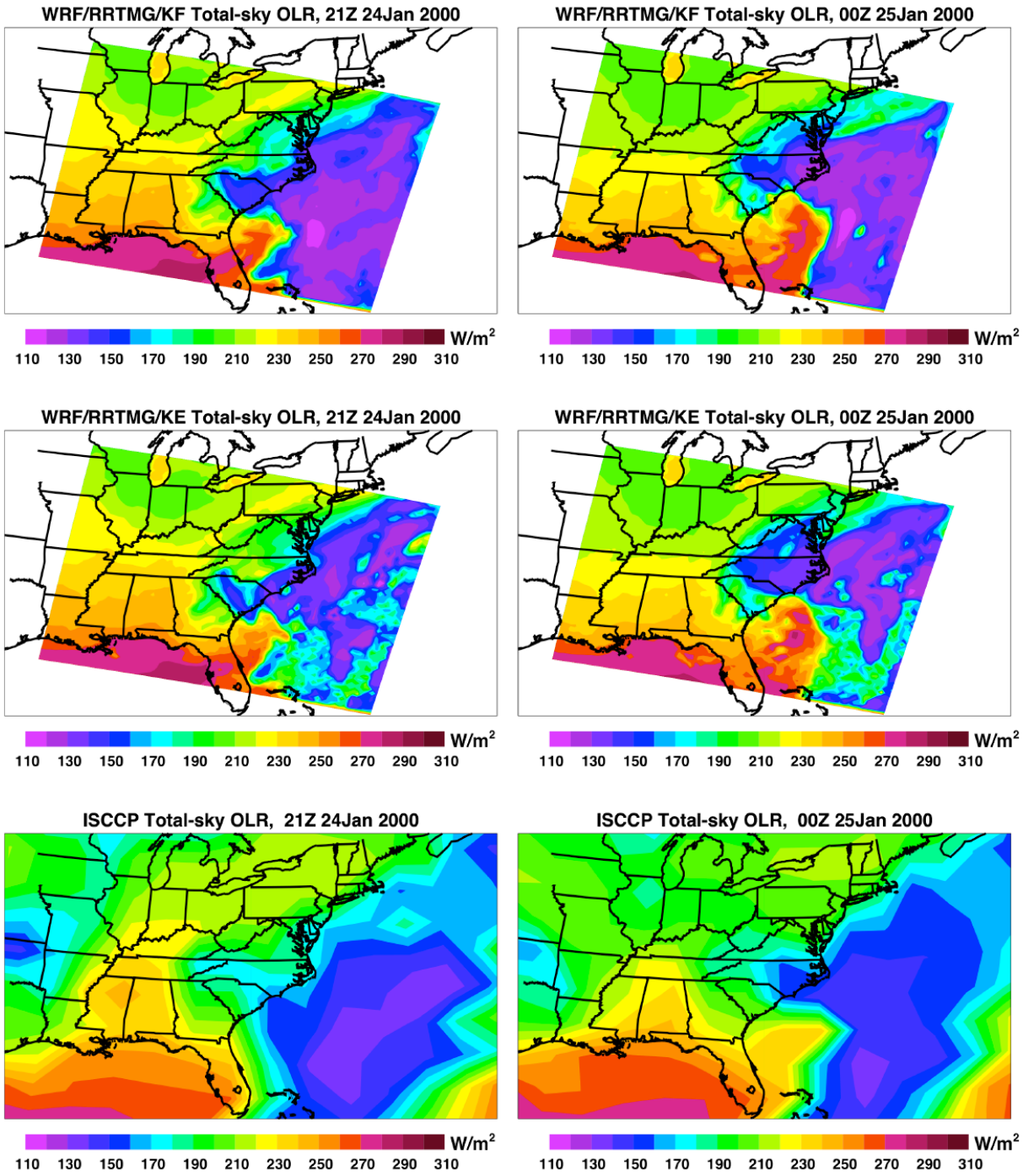

Figure 14. Total outgoing longwave radiation at 21 UTC 24 Jan 2000 (left) and at 00 UTC 25 Jan 2000 (right) as simulated by WRF with the RRTMG radiation and using the Kain-Fritsch ETA convection (top panels), the MIT/Emanuel convection and cloud schemes (center panels) and as measured by ISCCP (bottom panels). Note that the boundaries of the simulated WRF grid are smaller than the geographic area shown in each plot.

During the course of this project, collaborative posters were presented at the DOE Climate Change Prediction Program (CCPP) Science Team Meeting on 7-9 April 2009 and at the DOE Regional and Global Climate Modeling Program Science Team Meeting on 29 March – 2 April 2010. These posters summarized the research on the effect of the MIT and AER physics on the simulated convection and intra-seasonal oscillations in the NCAR climate model. Finally, a journal article summarizing the results of this project titled "Impacts of the AER Radiation and MIT Convection on the Water Cycle Simulated by CAM3.5" authored by B. Yang, K. Emanuel, W.R. Boos and M.J. Iacono will be submitted for publication in Fall 2010.

7. References

Betts, A.K., and C. Jacob, Evaluation of the diurnal cycle of precipitation, surface thermodynamics, and surface fluxes in the ECMWF model using LBA data, *J. Geophys. Res.*, *107,* doi:10.1029/2001JD000427, 2002.

Bony, S., and K.A. Emanuel, A parameterization of the cloudiness associated with cumulus Convection: Evaluation using TOGA COARE data. *J. Atmos. Sci*., 58, 3158-3183, 2001.

Emanuel, K.A., A scheme for representing cumulus convection in large scale models. *J. Atmos. Sci.*, 48, 2313–2335, 1991.

Emanuel, K.A., and M. Zivkovic-Rothman, Development and evaluation of a convection scheme for use in climate models, *J. Atmos. Sci*., 56, 1766-1782, 1999.

Iacono, M.J., J.S. Delamere, E.J. Mlawer, S.A. Clough, Evaluation of upper tropospheric water vapor in the NCAR community climate model (CCM3) using modeled and observed HIRS radiances, *J. Geophys. Res.*, **108(D2)**, 4037, doi:10.1029/2002JD002539, 2003.

Iacono, M.J., J.S. Delamere, E.J. Mlawer, M.W. Shephard, S.A. Clough, and W.D. Collins, Radiative forcing by long-lived greenhouse gases: Calculations with the AER radiative transfer models, *J. Geophys. Res.*, 113, D13103, doi:10.1029/2008JD009944, 2008.

Iacono, M.J., and T.R. Nehrkorn, Assessment of Radiation Options in the Advanced Research WRF Weather Forecast Model, Poster presentation at the First Atmospheric System Research Science Team Meeting, Bethesda, Maryland, March 15-18, 2010.

Lin, Z., D.A. Randall, and L.D. Fowler, Diurnal variability of the hydrologic cycle and radiative fluxes: Comparisons between observations and a GCM, *J. Climate*, 13, 4159-4179, 2000.

Yang, B., K.A. Emanuel, W.R. Boos and M.J. Iacono, Impacts of the AER radiation and MIT convection on the water cycle simulated by CAM3.5, in preparation, 2010.

Zhang, G.J. and N.A. McFarlane, Sensitivity of climate simulations to the parameterization of cumulus convection in the Canadian Climate Centre general circulation model. *Atmos. Ocean*., 33, 407-446, 1995.